Chinese Chemical Letters 37 (2026) 111344

Contents lists available at ScienceDirect

Chinese Chemical Letters

journal homepage: www.elsevier.com/locate/cclet

Zwitterionic poly(ionic liquid)-induced fast structural diffusion electrolytes for lithium metal batteries

Haiyang Liao[a], Tiemin Xiao[a], Tengfei Zhang[b], Chiam Wen Liew[c,*], Xiaofei Duan[a], Jiayi Su[a], Hongjin Kuang[a], Xiaolong Feng[a], Ting Li[d], Yongqi Zhang[b,*]

[a] School of Mechanical Engineering, Hunan University of Technology, Zhuzhou 412007, China
[b] Institute of Fundamental and Frontier Sciences, University of Electronic Science and Technology of China, Chengdu 611731, China
[c] Department of Physical Science, Faculty of Applied Sciences, Tunku Abdul Rahman University of Management and Technology, Jalan Genting Kelang, Kuala Lumpur 53300, Malaysia
[d] New Powertrain Development Division, Chongqing Chang'an Automobile Co., Ltd., Chongqing 401133, China

ARTICLE INFO

Article history:
Received 19 January 2025
Revised 16 May 2025
Accepted 19 May 2025
Available online 20 May 2025

Keywords:
Polymer electrolyte
Lithium metal battery
In-built method
Zwitterionic poly(ionic liquid)
Diffusion mechanism

ABSTRACT

Poly(ethylene oxide) (PEO) electrolytes present a promising option for next-generation solid-state high-energy-density batteries. However, the poor ionic conductivity and inefficiency transference number pose significant barriers to its broader application. Herein, an in-built synthesis of poly(ethylene oxide) with zwitterionic poly(ionic liquid) composite electrolyte (PEO/Zwit PIL) is employed by a thio-lene click reaction. The introduction of Zwit PIL can help the composite electrolyte fully dissociation lithium salts and optimize the solvation structure. Molecular dynamics simulations elucidate fast Li^+ transport through a structural diffusion mechanism upon the addition of Zwit PIL to the composite electrolyte, simultaneously facilitating a high ionic conductivity and transference number. The composite electrolyte also demonstrates a high self-adhesive to construct a robust and tough electrode-electrolyte interface. The assembled full cell (LiFePO4||PEO-Zwit PIL||Li) exhibits a discharge capacity of 153 mAh/g at 60 °C and highly stable cyclic performance up to 200 cycles at 0.2 C. The employment of Zwit PIL within PEO for novel solid-state electrolytes furnishes an alternative approach to the design of high-performance, next-generation, sustainable batteries.

© 2026 Published by Elsevier B.V. on behalf of Chinese Chemical Society and Institute of Materia Medica, Chinese Academy of Medical Sciences.

The development of high-energy-density energy storage technology has necessitated the exploration of next-generation anode materials. Lithium metal is regarded as the optimal anode material for lithium-ion batteries, owing to its low electrochemical potential (−3.04 V *vs.* SHE) and high theoretical capacity (3860 mAh/g) [1–4]. However, the highly reactive nature of lithium metal poses significant safety concerns due to various side reactions [5,6]. Therefore, the development of compatible electrolyte materials is essential to ensure safety and long-term cycling. Polymer electrolytes (PE) have emerged as the preferred choice for lithium-metal batteries, owing to their significant advantages in enhanced safety, softness and compatibility with lithium metal [7–10].

Poly(ethylene oxide) (PEO) and co-polymers represent the most intensively studied. Their inherent structure, characterized by the strong coordination of metal ions, gives rise to a crucial challenge. Specifically, it is difficult to achieve high ionic conductivity and Li^+ transference number [11–13]. Researchers have put forward several strategies, including introducing loosely-coordinating units, implementing copolymerization, and cross-linking [14–16]. However, there are difficulties in increasing the Li^+ transference number beyond 0.5. Another approach aimed at maximizing the Li^+ transference number involves the use of polyanionic materials. Anions are confined by the polymer backbone, and cation conduction takes the lead. This helps to overcome the anion concentration gradient, causing the cation mobility to approach unity [17–19]. However, such single-ion conductors exhibit extremely low ionic conductivity, even when blended with PEO-based PEs. Recently, a novel class of polymer electrolytes known as zwitterionic polymeric ionic liquid (Zwit PIL) has emerged. These materials show promise as potential solid-state solvents for lithium salts [20,21]. Interestingly, owing to the distinct Li-Zwit PIL coordination structure, the ionic conductivity is directly proportional to the lithium salt's concentration. This stands in contrast to conventional PEO-based PEs that operate *via* a "hopping" diffusion mechanism [22–24]. Consequently, there is great promise in obtaining electrolytes with both high ionic conductivity and transference num-

* Corresponding authors.
E-mail addresses: liewcw@tarc.edu.my (C.W. Liew), yqzhang@uestc.edu.cn (Y. Zhang).

https://doi.org/10.1016/j.cclet.2025.111344
1001-8417/© 2026 Published by Elsevier B.V. on behalf of Chinese Chemical Society and Institute of Materia Medica, Chinese Academy of Medical Sciences.

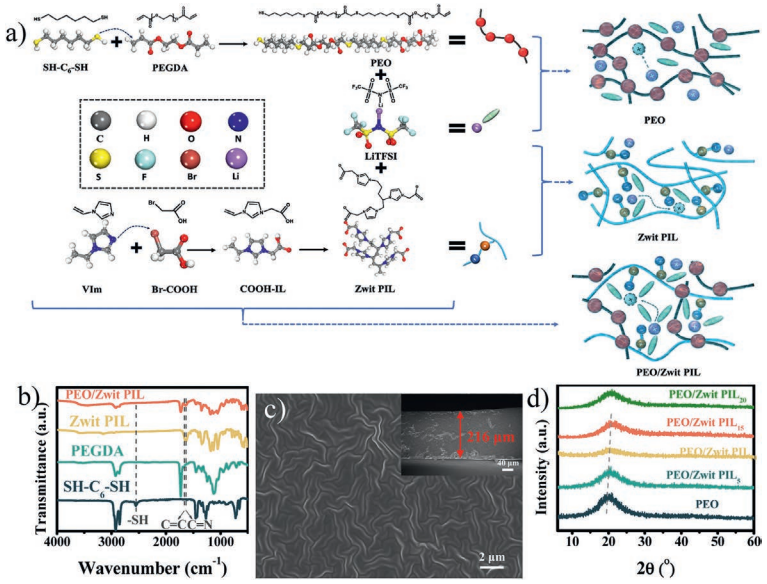


Fig. 1. (a) Schematic preparation of the PEO-based electrolyte. (b) FTIR of the monomer and electrolytes. (c) SEM image of the PEO/Zwit PIL_{10}, insert is its cross-section. (d) XRD patterns of the electrolytes.

bers by compositing the Li-Zwit PIL system with PEO. However, the Li^+ diffusion mechanism in such composite electrolytes has been scarcely reported. Given the promising applications of composite electrolytes, a thorough understanding of their fundamental mechanism could open the door to the development of advanced solid-state electrolytes based on the Li-PEO-Zwit PIL framework.

In this paper, composite electrolytes containing PEO and Zwit PIL (PEO/Zwit PIL) were synthesized through click polymerization. Upon incorporation into PEO electrolytes, the Zwit PIL can integrate into the coordination configuration of lithium, resulting in the formation of Li-Zwit PIL-PEO complexes. The interaction between Zwit PIL and PEO induces a solvent structure with weakened PEO-Li interactions, facilitating enhanced Li^+ transportation. Interestingly, the presence of Zwit PIL in the PEO-based electrolyte alters the diffusion behavior, leading to enhanced structural diffusion of Li^+ transportation. The in-built composite electrolyte directly forming onto the electrodes exhibits robust adhesion and establishes a secure electrolyte-electrode interface. Therefore, lithium iron phosphate cells ($LiFePO_4$||Li) with PEO-Zwit PIL as solid-state electrolytes exhibit good electrochemical performances. This PEO-based solid-state electrolyte containing Zwit PIL opens an avenue for developing safer high-energy-density batteries.

The preparation process and the structures of PEO/Zwit PIL are illustrated in Fig. 1a. In the thiol-olefin click polymerization process, the -SH terminal group in 1,6-hexanedithiol ($SH-C_6-SH$) engages in a chemical reaction with the terminal C=C group in poly(ethylene glycol) diacrylate (PEGDA), resulting in the formation of a polymer bonded by C-S-C. Therefore, the chemical structures of the monomer and the polymers were verified *via* Fourier transform infrared spectroscopy (FTIR), as shown in Fig. 1b. The characteristic bands associated with the C=C group at 1638 cm^{-1} and the -SH group at 2450 cm^{-1} disappeared from the FITR of PEO, instead, the new characteristic band corresponding to C-S-C at 950 cm^{-1} emerged, indicating the occurrence of a thiol-olefin click reaction [25,26]. Notably, both the broadband at 1640 cm^{-1} attributed to C=N in Zwit PIL and the characteristic band originally belonging to PEO are similarly found in the FTIR of PEO/Zwit PIL [27], suggesting that the composite electrolyte was successfully prepared.

Electrolyte morphology was investigated using scanning electron microscope (SEM), as shown in Fig. 1c and Fig. S3 (Supporting information). PEO/Zwit PIL_{10} electrolyte demonstrate a dense and defect-free morphology with the thickness of 223 μm (Fig. 1c). The morphology of the other component electrolytes can be found in Figs. S3a-d, which are similar to the morphology and thickness of PEO/Zwit PIL_{10}. This indicates that Zwit PIL has better compatibility with PEO. Notably, As Zwit PIL cannot form a film by itself, electrospun PVDF-HFP was employed as the structure framework. It can fill the gaps in the PVDF-HFP fiber membrane, yielding a flat morphology with thickness of 53 μm (Fig. S3e).

The impact of incorporating Zwit PIL on the crystalline phase of PEO was examined by X-ray diffraction (XRD) measurement (Fig. 1d). The PEO-based electrolyte exhibits a distinctive bun-shaped crystalline band at 20°, suggesting a state of semi-crystallinity. The incorporation of Zwit PIL results in a reduction in the intensity of the crystalline bands of PEO and a shift of the band position to a higher degree. Noteworthy, the crystallinity shows a slight increase (does not exceed that of pure PEO) once the Zwit PIL content exceeds 10%. The decreased crystallinity can be attributed to the role of a limited amount of Zwit PIL, which functions as a plasticizer for PEO, diminishing the intermolecular interactions within the PEO chains [28]. Once the content surpasses a critical threshold, compatibility issues lead to phase separation, allowing PEO chain segments to re-establish close contact. The reduction in crystallinity promotes expansion of the amorphous region, consequently culminating in a decline in the T_g, as evidenced in Fig. S4 (Supporting information). Moreover, PEO/Zwit PIL maintains sufficient strength despite T_g decrease (Fig. S5 in Supporting information).

The electrochemical stability of the electrolyte is essential to ensure the battery's surety. In Fig. 2a, all curves rise sharply at a certain point after maintaining a low current as the voltage increases, indicating the decomposition of the electrolyte. Accordingly, the electrochemical stability of PEO is observed at 4.3 V *vs.* Li/Li^+, while that of Zwit PIL occurs at 4.7 V *vs.* Li/Li^+. The incorporation of Zwit PIL results in an enhancement in the electrochemical stability, reaching the maximum value of 4.8 V at the 10% of Zwit PIL content, suggesting potential application in lithium metal batteries. The electrochemical stability for other Zwit PIL composite electrolytes can be found in Fig. S6 (Supporting information).

The ionic conductivity of the electrolytes was investigated using electrochemical impedance spectroscopy (EIS), as shown in Fig. S7 (Supporting information). The calculated (by Eq. S1 in Supporting information) minimum ionic conductivity is pure PEO electrolyte,

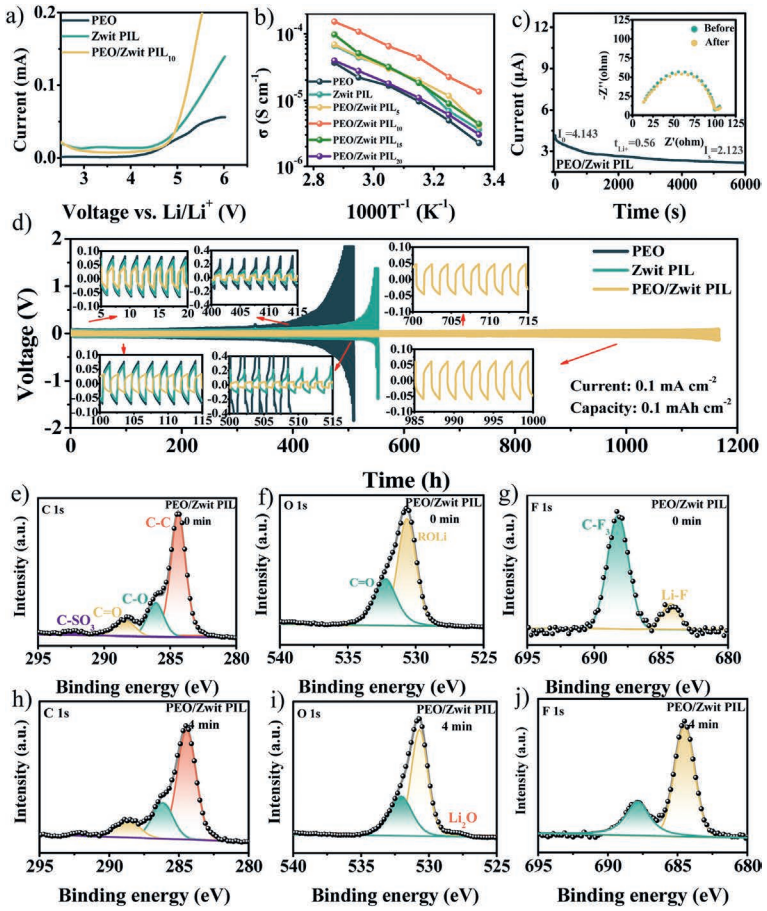


Fig. 2. (a) LSV curves of the electrolytes. (b) The dependence of ionic conductivity on temperatures. (c) Chronoamperometric tests of the PEO/Zwit PIL electrolytes under polarization potential (10 mV) and the insert shows the Nyquist impedance spectra before and after polarization. (d) Galvanostatic cycling curves of symmetrical cells at 0.1 mA/cm^2. (e-g) Initial deep sputtering of XPS test on C 1s, O 1s, and F 1s spectra, (h-j) 4 min-later deep sputtering of XPS test on C 1s, O 1s, and F 1s spectra.

only giving 2.26×10^{-6} S/cm. Upon incorporation of Zwit PIL, the ionic conductivity experiences improvement (Fig. S8 in Supporting information). The maximum ionic conductivity is PEO/Zwit PIL$_{10}$ with value of 6.85×10^{-5} S/cm, superior to those PEO-bsaed and PEO/inorganic composite electrolytes [29–32]. The improvement can be attributed to the ability of lithium ions and Zwit PIL to form IL-like low melting ion pairs. The COO^- anion in Zwit PIL exerts a significant electrostatic influence on Li^+ cation, which can weaken the strong coupling between the Li^+ and PEO segment, thereby facilitating a more accessible release of Li^+. The ionic conductivity depends on temperature as shown in Fig. 2b. The ion conductivity of the PEO/Zwit PIL$_{10}$ electrolyte exhibits a marked increase with rising temperature, suggesting that the mobility of ions becomes significantly more dynamic. Kinetics of ion transport were further explored by fitting Eq. S2 (Supporting information). The calculated active energy (E_a) can be found in Fig. S9 (Supporting information). A minimum E_a value of 0.049 eV is obtained at 10 % Zwit PIL (Considering its superior ionic conductivity, PEO/Zwit PIL$_{10}$ will be selected as the representative composite electrolyte for forthcoming performance tests and denoted as PEO/Zwit PIL).

Ionic conductivity measures the ease of migration of all free ions (including cations and anions). Ideal ionic mobility within lithium metal batteries necessitates the effective migration of Li^+ while impeding the other ions. The lithium-ion transference number (t_{Li^+}) was evaluated and calculated by Eq. S3 (Supporting information). The calculated t_{Li^+} of PEO/Zwit PIL (Fig. 2c) composite electrolytes is 0.56, higher than that of pure PEO (Fig. S10a in Supporting information) and Zwit PIL (Fig. S10b in Supporting information). The improved t_{Li^+} for PEO/Zwit PIL can be attributed to the synergistic effect between PEO and Zwit PIL, alongside the single-ion conduction of Zwit PIL.

Apart from the ionic conductivity and Li^+ mobility, the stability of the electrolyte-electrode interface is also of critical importance, which plays a significant role in influencing the longevity of the battery. The investigation of interfacial stability was conducted through cyclic deposition/stripping under specific current density (0.1 mAh/cm^2) and areal capacity conditions (0.1 mAh/cm^2). All the measurements were conducted at 60 °C. As depicted in Fig. 2d, the PEO/Zwit PIL demonstrates a minimal overpotential of 30 mV and maintains stable cycling performance for as long as 1000 h. In comparison, the PEO and Zwit PIL exhibit unstable polarization after 400 h and 500 h, respectively. Moreover, the PEO/Zwit PIL electrolyte is able to deliver exceptional rate performance and stable high rate cycling, as shown in Figs. S11a and b (Supporting information), which is superior to the rate performance of other solid-state PEO-based electrolytes reported in the literature [33–35]. The results are ascribed to robust solid-state interface (SEI) [36,37] caused by the enhanced compatibility between the PEO/Zwit PIL composite electrolyte and lithium electrode, which is evidence by compatibility testing (Fig. S12 in Supporting information). The improved compatibility is associated with electrolyte and electrode contact. The presence of -COOLi in Zwit PIL and the abundance of C–O–C in PEO can facilitate the formation of hydrogen bonds with lithium metal surface, resulting in a strong adhesive connection (Fig. S13 and Video S1 in Supporting information). The morphology of the lithium electrode after cycling was further observed by SEM

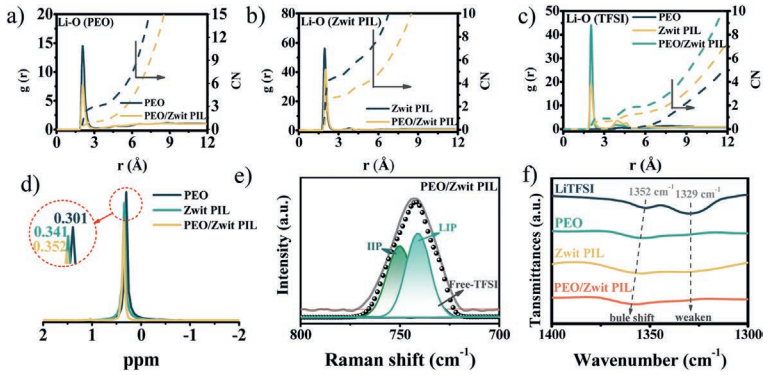


Fig. 3. RDF curves of Li-O: (a) PEO, (b) Zwit PIL, (c) PEO/Zwit PIL; spectral testing of the electrolytes: (d) ss-NMR spectra, (e) Raman spectra, (f) FTIR spectra.

(Figs. S14 and S15 in Supporting information), and it is found that unlike pure PEO and Zwit PIL, the lithium metal of PEO/Zwit PIL not only has a flat surface but also maintains a compact structure in its cross-section, which suggests that the growth of dendrites is inhibited.

Furthermore, X-ray photoelectron spectroscopy (XPS) depth profiling was employed to investigate the SEI composition. The C–O peak at the C 1s and ROLi peak at O 1s indicate products resulting from the decomposition of PEO (Figs. 2e and f), which is responsible for the loose-structure for electrolyte-lithium interface [38]. The C-SO_3 signal at C 1s and the CF_3 peak at F 1s suggest the presence of trapped $TFSI^-$ (Figs. 2e and g) [39]. The LiF peak detected at F 1s is associated with the decomposition of $TFSI^-$ (Fig. 2g), which is primarily responsible for the stable interface. After a 4-min sputtering time, the C=O and ROLi signals in both the PEO/Zwit PIL (Figs. 2h–j) and Zwit PIL electrolytes (Fig. S16 in Supporting information) exhibited minimal changes. Instead, there was a notable increase in the LiF component, alongside the formation of Li_2O and Li_3N (Fig. S17 in Supporting information), which are associated with the SEI densification. This behavior contrasts sharply with the SEIs observed in PEO electrolytes (Fig. S8), where they are dominated by electrolyte decomposition products.

To more accurately probe the influence of the electrolyte-electrode stabilization interface, molecular dynamic (MD) simulations were employed to investigate the transport mechanism and chemical environments associated with Li^+. It is important to highlight that the structure of PEO was utilized for modeling instead of the PEGDA. This is because the segment of the molecule that engages in significant interactions remains the ethylene oxide (EO) group. The quantification of molecules in each system can be referred to Table S1 (Supporting information). The radial distribution function ($g(r)$) within 30 ns to analyze complex competitive interactions. In the PEO electrolyte, the PEO segment occupied the solvation sheath with relatively high $g(r)$ (Fig. 3a), and the $TFSI^-$ involved in the solvation sheath shows a reduced proportion of $g(r)$ (Fig. 3c), meaning that Li^+ is mainly coupled with PEO segments (Fig. S19a in Supporting information) [40]. In the pure Zwit PIL electrolyte, Zwit PIL forms a strongly coordinated solvation sheath with Li^+ (Fig. 3b and Fig. S19b in Supporting information) [41], and, $TFSI^-$ exhibits a weakly coordinating interaction with Li^+ (Fig. 3c). In the PEO/Zwit PIL electrolyte, the interaction of Li^+ with PEO and Zwit PIL weakened (Figs. 3a and b, Fig. S19c in Supporting information), suggesting that the introduction of the Zwit PIL induced competitive interactions among PEO, Zwit PIL, and $TFSI^-$. The result reveals that Li^+ primarily engages directly with the segments of the polymer chains in the pure PEO and Zwit PIL electrolyte. This coupling introduces a Li^+ transport mechanism that corresponds with the “hopping” diffusion. In contrast, the emergence of competitive interactions between Zwit PIL and PEO within the PEO/Zwit PIL electrolyte results in a weak inter-coordination between Li-Zwit PIL-PEO so that $TFSI^-$ bridging coordination with Li^+. In this coupled case, Li^+ is both weakly coordinated with the polymer segment and interacting with $TFSI^-$. Consequently, the Li^+ transportation comes more decoupled from the polymer segment. The diffusion mechanism of Li^+ in the PEO/Zwit PIL is very similar to the structural diffusion mechanism, *i.e.*, the ligand is a partial exchange of ligands during the Li^+ transport. The structure diffusion mechanism can be studied by tracing the coordinated anions ($TFSI^-$) of a given Li^+ during its diffusion. When conceptualizing a coordination shell as a "cage", we can quantitatively analyze the restructuring of this cage and its relationship to the diffusion processes of Li^+. To facilitate this analysis, we define a "cage-restructure correlation function" ($C(t)$, Eq. S4 in Supporting information), which quantifies the time interval between the formation of an initial cage and the establishment of a new cage (Fig. S20 in Supporting information). The structural diffusion mechanism is recognized as a short convergent $C(t)$ curve (Fig. S21a in Supporting information), due to ion diffusion occurring *via* the restructuring of the cage. Density functional theory (DFT) calculations (Fig. S12b in Supporting information) shows that the Li-Zwit PIL-PEO solvation structure exhibits a minimum binding energy of 0.78 eV (calculated from Eq. S3), indicating that the introduction of Zwit PIL diminishes the interaction between Li^+ and PEO segments. The low-coupling solvation structure favors Li^+ transport, as evidence by mean square displacement (MSD) and last MSD (Figs. S21c and S22 in Supporting information).

Solid-state nuclear magnetic resonance (ss-NMR) and spectroscopic evaluations validated the solvation structure found in the MD simulations. In the ^7Li NMR spectra (Fig. 3d), different from pure PEO (0.301 ppm) and Zwit PIL (0.341), lithium nuclei in PEO/Zwit PIL electrolyte display a reduced shielding effect accompanied by a minor shift (0.352 ppm), suggesting that the introduction of the Zwit PIL disrupts the binding interactions between Li-PEO [42]. ^{19}F NMR spectra of $TFSI^-$ further confirms that Li^+ exhibits strong coordination with $TFSI^-$ in the PEO/Zwit PIL electrolyte (Fig. S23 in Supporting information). The solvation structures of Li^+ were further examined using Raman spectroscopy. The peaks observed at ~738, 742, and 752 cm^{-1} correspond to distinct species: $TFSI^-$ free ions (Free-TFSI), loose ion pairs (LIP), and intimate ion pairs (IIP), respectively (Fig. 3e) [43,44]. Departing from PEO (Free-TFSI-dominated, Fig. S24a in Supporting information) and Zwit PIL (LIP-dominated, Fig. S24b in Supporting information), LIP and IIP in the PEO/Zwit PIL become the dominant structures which percentage of 50% and 44% (Table S2 in Supporting information), respectively, reflecting a more pronounced contact interaction between Li^+ and $TFSI^-$ (Fig. 3e). FTIR spectroscopy was further measured to validate the interaction between LiTFSI and polymer segment (Fig. 3f). The band at 1352 cm^{-1} in the LiTFSI, asso-

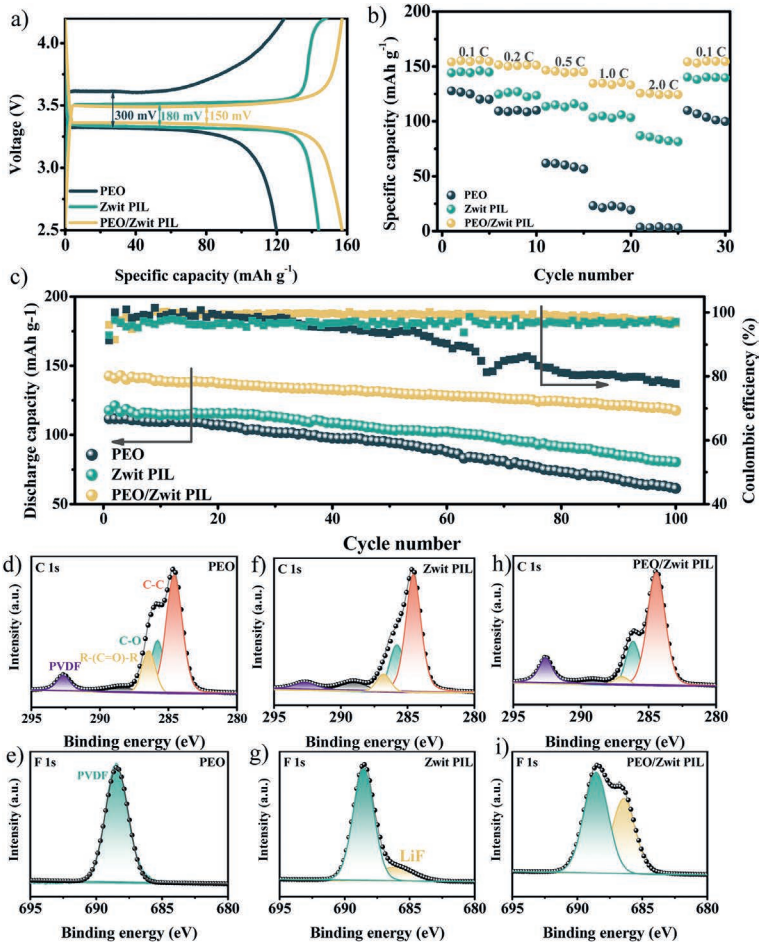


Fig. 4. Electrochemical performance of cells with different electrolytes at 60 °C: (a) Charge/discharge performances. (b) Rate behavior. (c) Cycling stability of the cell based on different electrolyte at voltage of 4.3 V. C 1s and F 1s spectra of cycled $LiFePO_4$ full cells with different electrolytes: (d, e) PEO; (f, g) Zwit PIL; (h, i) PEO/Zwit PIL.

ciated with the O=S=O group, exhibited a blueshift (the shifts for Zwit PIL and PEO/Zwit PIL > pure PEO). Additionally, the bands of S-N-S at 1332 cm^{-1} are gradual attenuation, suggesting that the Zwit PIL and PEO/Zwit PIL engage in interactions with the $TFSI^-$. The lithium ion diffusion coefficients calculated from EIS method [45] finally validate the correctness of the MSD results in the MD simulations, suggesting that the low coupling interactions enhance Li^+ transport (Fig. S25 in Supporting information).

To evaluate the electrochemical performance of PEs in full lithium metal batteries, $LiFePO_4$||Li cells were assembled and cycled at 60 °C. The active material loading on the cathode is ~3.2 mg/cm^2. Fig. 4a shows the charge-discharge curve of various electrolytes at a 0.1 C. The PEO-based cell demonstrates a discharge capacity of only 120 mAh/g. In contrast, the Zwit PIL and PEO/Zwit PIL-based cells exhibit superior discharge capacities, reaching 142 and a maximum of 155 mAh/g, respectively. These findings indicate that the PEO/Zwit PIL cells exhibit enhanced charge/discharge performance. Owing to its high ionic conductivity, the PEO/Zwit PIL-based cell is capable of working at room temperature (30 °C, tested in July), demonstrating a capacity of 135 mAh/g (Fig. S26 in Supporting information) with 85 % 100-cycle capacity retention (Fig. S27 in Supporting information). The rate performance of the cells was further tested from 0.1 C to 2.0 C (Fig. 4b). The $LiFePO_4$||PEO/Zwit PIL||Li cell displays superior rate capability than both PEO-based (<100 mAh/g at 0.5 C) and Zwit PIL-based cell (<100 mAh/g at 1.0 C) at 60 °C. The specific discharge capacity maintains 125 mAh/g at 2.0 C, which is superior to most of the previous reports based on PEO-based electrolytes (Table S3 in Supporting information). Furthermore, remarkable cycling performance (Fig. S28a in Supporting information) and stable EIS (Fig. S28b in Supporting information) suggest that PEO/Zwit PIL electrolytes have the potential application in next-generation solid-state polymer lithium-metal batteries. To demonstrate the performance at elevated voltage and high loading, the $LiFePO_4$-based cell (>3 mAh/cm^2) was cycled at 0.2 C within a wide voltage range of 4.3–2.5 V. The cell with PEO/Zwit PIL electrolyte maintains 83 % of its initial capacity after 100 cycles which surpasses the performance of the Zwit PIL and PEO electrolyte. Their capacity retention is only 68 % and 55 %, respectively (Fig. 4c). The composition of the cathode-electrolyte interface after cycling was further investigated. The C 1s spectra for PEO electrolyte reveals significant intensity of R-(C=O)-R (287.5 eV) and C=O (288.5 eV), suggesting that partial decomposition of the electrolyte occurs at the cathode interface (Fig. 4d). The F 1s spectra shows a negligible presence of LiF (Fig. 4e). These indicate that an unstable cathode-electrolyte in the PEO-based cell [46,47]. The phenomenon is alleviated in the Zwit PIL-based cell, where the R-(C=O)-R and C=O decreasing, and LiF emerged (Figs. 4f and g). Much differently, intensity of C–C (284.5 eV, from carbon conducting agent) and PVDF (291.5 eV, from PVDF binder) instead of R-(C=O)-R and C=O dominate the C 1s spectra in the PEO/Zwit PIL-based cell (Figs. 4h and i). Additionally, LiF shows a marked increase. These results suggest that less electrolyte decomposition occurs in the cell with PEO/Zwit PIL electrolyte, and this allows maintenance of the interfacial stability of the cathode-lectrolyte.

In summary, a PEO/Zwit PIL composite electrolyte is synthesized *via in-situ* technique on the surface of lithium metal through click polymerization. Incorporating Zwit PIL into the PEO matrix facilitates competitive coordination with Li^+, reducing the PEO-Li interaction. This modification not only promotes the coordination between $TFSI^-$ and Li^+ but also optimizes the diffusion mechanism, ultimately leading to improved ionic conductivity. Additionally, the COO^- in Zwit PIL has been observed to facilitate the release of free Li^+ from LiTFSI, thereby enhancing t_{Li+}. The composite electrolyte exhibits robust interfacial adhesion with the lithium electrode, which is beneficial for stabilizing the formation of the SEI layer. The remarkable electrolyte properties of PEO/Zwit PIL facilitate impressive electrochemical performance at 60 °C. This advancement is pivotal in addressing the challenges associated with the development of solid-state PEs.

CRediT authorship contribution statement

Haiyang Liao: Writing – original draft, Methodology, Conceptualization. **Tiemin Xiao:** Formal analysis, Data curation. **Tengfei Zhang:** Methodology, Investigation, Data curation. **Chiam Wen Liew:** Writing – review & editing, Supervision. **Xiaofei Duan:** Methodology, Investigation. **Jiayi Su:** Resources, Investigation, Formal analysis. **Hongjin Kuang:** Methodology, Formal analysis, Data curation. **Xiaolong Feng:** Methodology, Investigation, Data curation. **Ting Li:** Methodology, Data curation. **Yongqi Zhang:** Writing – review & editing, Supervision, Funding acquisition.

Declaration of competing interest

The authors declare that they have no known competing financial interests or personal relationships that could have appeared to influence the work reported in this paper.

Acknowledgments

This work was supported by the link project of the National Science Foundation of China (Nos. 22379020 and 22209020), Natural Science Foundation of Hunan Province (No. 2023JJ50171). The authors appreciate Tingchuan Zhou from Analysis and Testing Center, University of Electronic Science and Technology of China, for technical support.

Supplementary materials

Supplementary material associated with this article can be found, in the online version, at doi:10.1016/j.cclet.2025.111344.

References

[1] D. Cai, X. Wu, J. Xiang, et al., Chem. Eng. J. 424 (2021) 130522.
[2] R. Khurana, J.L. Schaefer, L.A. Archer, G.W. Coates, J. Am. Chem. Soc. 136 (2014) 7395–7402.
[3] H. Wang, Q. Wang, X. Cao, et al., Adv. Mater. 32 (2020) 2001259.
[4] X. Fan, K. Xiang, W. Zhou, et al., Carbon Ener. 6 (2024) e536.
[5] H. Wu, H. Jia, C. Wang, J.G. Zhang, W. Xu, Adv. Ener. Mater. 11 (2020) 2003092.
[6] S. Wang, P. Xiong, J. Zhang, G. Wang, Ener. Storage Mater. 29 (2020) 310–331.
[7] R. Li, H. Hua, Y. Zeng, et al., J. Ener. Chem. 64 (2022) 395–403.
[8] M. Nakayama, S. Wada, S. Kuroki, M. Nogami, Ener. Environ. Sci. 3 (2010) 1995.
[9] C. Wang, R. Li, P. Chen, et al., J. Mater. Chem. A 9 (2021) 4758–4769.
[10] J. Feng, L. Wang, Y. Chen, et al., Nano Converg. 8 (2021) 1–12.
[11] Y. Ji, Y.H. Zhang, F.N. Shi, L.N. Zhang, J. Colloid Interf. Sci. 629 (2023) 492–500.
[12] S. Xu, Z. Sun, C. Sun, et al., Adv. Funct. Mater. 30 (2020) 2007172.
[13] Y. Zhang, W. Lu, L. Cong, et al., J. Power Sources 420 (2019) 63–72.
[14] H. Wang, T. Hou, H. Cheng, et al., J. Ener. Chem. 71 (2022) 218–224.
[15] F. Wu, K. Zhang, Y. Liu, et al., Ener. Storage Mater. 33 (2020) 26–54.
[16] R. Li, H. Hua, X. Yang, et al., Ener. Environ. Sci. 17 (2024) 5601–5612.
[17] J. Atik, D. Diddens, J.H. Thienenkamp, et al., Angew. Chem. Int. Ed. 60 (2021) 11919–11927.
[18] F. Chen, X. Wang, M. Armand, M. Forsyth, Nat. Mater. 21 (2022) 1175–1182.
[19] L. Liu, T. Wang, L. Sun, et al., Ener. Environ. Mater. 7 (2023) e12580.
[20] F. Ma, Z. Zhang, W. Yan, et al., ACS Sustain. Chem. Eng. 7 (2019) 4675–4683.
[21] X. Wei, J. Zhou, X. Wang, et al., Chem. Eng. J. 498 (2024) 155614.
[22] R. Cao, K. Chen, Y. Cui, et al., Chin. Chem. Lett. 34 (2024) 108711.
[23] K. Yin, Z. Zhang, L. Yang, S.I. Hirano, J. Power Sources 258 (2014) 150–154.
[24] Q. Liu, L. Li, G. Liu, et al., J. Power Sources 592 (2024) 233897.
[25] L. Liang, W. Yuan, X. Chen, H. Liao, Chem. Eng. J. 421 (2021) 130000.
[26] Y. Ren, J. Guo, Z. Liu, et al., Sci. Adv. 5 (2019) eaax0648.
[27] H. Liao, J. Su, J. Han, et al., Macromol. Rapid Comm. 45 (2024) 2300613.
[28] J. Tan, X. Ao, A. Dai, et al., Ener. Storage Mater. 33 (2020) 173–180.
[29] L. Chen, Y. Li, S.-P. Li, et al., Nano Ener. 46 (2018) 176–184.
[30] C. Li, S. Deng, W. Feng, et al., Small 19 (2023) 2300066.
[31] X. Li, S. Liu, J. Shi, et al., Chem. Eng. J. 468 (2023) 143795.
[32] Z. Wang, S. Wang, A. Wang, et al., J. Mater. Chem. A 6 (2018) 17227.
[33] L. Zou, K. Shi, H. Liu, et al., Chem. Eng. J. 465 (2023) 142794.
[34] Z. Chen, J. Li, F. Qiu, et al., J. Mater. Chem. A 10 (2022) 14849–14856.
[35] L. Gao, W. Jiang, X. Zhang, et al., Chem. Eng. J. 479 (2024) 147822.
[36] H. Liao, W. Zhong, C. Li, et al., J. Ener. Chem. 89 (2024) 565–578.
[37] X. Lin, S. Xu, Y. Tong, et al., Mater. Horiz. 10 (2023) 859–868.
[38] X. Jiao, J. Wang, G. Gao, et al., ACS Appl. Mater. Interfaces 13 (2021) 60054–60062.
[39] X. Zhu, Z. Fang, Q. Deng, et al., ACS Sustain. Chem. Eng. 10 (2022) 4173–4185.
[40] Y. Xiao, X. Wang, K. Yang, et al., Ener. Storage Mater. 55 (2023) 773–781.
[41] H. Chang, W. Li, H. Liu, et al., Chem. Eng. J. 481 (2024) 148602.
[42] S. Kondou, M. Abdullah, I. Popov, et al., J. Am. Chem. Soc. 146 (2024) 33169–33178.
[43] T. Chen, Y. Liu, Z. Jin, et al., Giant 19 (2024) 100310.
[44] Y. Liu, Z. Jin, Z. Liu, et al., Angew. Chem. Int. Ed. 136 (2024) e202405802.
[45] X. Wang, H. Hao, J. LIu, T. Huang, A. Yu, Electrochim. Acta 56 (2011) 4065–4069.
[46] Y. Qian, P. Niehoff, M. Borner, et al., J. Power Sources 329 (2016) 31–40.
[47] J. Kwangeun, T. Yim, Rare Metals 40 (2021) 2793–2801.